Predicting Atlantic Basin Seasonal Tropical Cyclone Activity by 1 August

WILLIAM M. GRAY AND CHRISTOPHER W. LANDSEA

Department of Atmospheric Science, Colorado State University, Fort Collins, Colorado

PAUL W. MIELKE, JR.

Department of Statistics, Colorado State University, Fort Collins, Colorado

KENNETH J. BERRY

Department of Sociology, Colorado State University, Fort Collins, Colorado

(Manuscript received 6 March 1992, in final form 22 October 1992)

ABSTRACT

More than 90% of all seasonal Atlantic tropical cyclone activity typically occurs after 1 August. A strong predictive potential exists that allows seasonal forecasts of Atlantic basin tropical cyclone activity to be issued by 1 August, prior to the start of the active portion of the hurricane season. Predictors include June–July meteorological information of the stratospheric quasi-biennial oscillation (QBO), West African rainfall, the El Niño–Southern Oscillation (ENSO) as well as sea level pressure anomalies (SLPA), and the upper-tropospheric zonal-wind anomalies (ZWA) in the Caribbean basin.

Use of a combination of these global and regional predictors provides a basis for making cross-validated (jackknifed) 1 August hindcasts of subsequent Atlantic seasonal tropical cyclone activity that show substantial skill over climatology. This relationship is demonstrated in 41 years of hindcasts of the 1950–90 seasons. It is possible to independently explain more than 60% of the year-to-year variability associated with intense (category 3–4–5) hurricane activity. This is significant because over 70% of all United States tropical cyclone damage comes from intense hurricanes, and over 98% of intense hurricane activity occurs after 1 August.

Empirical evidence suggests that least sum of absolute deviations (LAD) regression yields substantially more improved cross-validated results than an analogous procedure based on ordinary least sum of squared deviations (OLS) regression. This improvement surprisingly occurs even with the squared Pearson product–moment correlation coefficient for which one might anticipate OLS regression to yield better cross-validated results than LAD regression.

1. Introduction

This paper investigates improved predictions of seasonal Atlantic tropical cyclone (TC) activity. While an earlier paper (Gray et al. 1992c) considers predictions from 1 December of the previous year, the present paper deals with the notably stronger predictive capabilities that are available each year by 1 August for making forecasts for the likely incidence of TC activity for the most active portion of the season during August–October.

Earlier work by the first author (Gray 1984a,b) demonstrates that seasonal predictability of Atlantic basin TC activity above that specified by climatology is feasible by the start of the hurricane season. Seasonal variations of several global and regional climate parameters are associated with strong season-to-season variations of cyclone activity in the Atlantic basin. Accurate seasonal predictions are possible through the use of these climate controls. Similar predictive relationships of this degree of accuracy are generally not available for the other global TC basins, wherein conditions for cyclone activity are more robust and where a monsoon trough (rather than easterly waves from Africa) is the primary component for TC formation. Cyclone activity in the other global cyclone basins is also not as seasonally concentrated as in the Atlantic, where the majority of intense hurricane activity occurs in the comparatively short 50-day period between 20 August and 10 October. This temporal focus of Atlantic TC activity allows for the concentration of seasonal forecast parameters on the single month of September. These forecast advantages are not available in the other ocean basins, wherein seasonal forecasting shows less potential skill (Chan 1991; Nicholls 1992).

Nine predictors can be used for 1 August Atlantic basin seasonal forecasts. These include the global-scale climatic factors of the stratospheric quasi-biennial oscillation (QBO) and the El Niño–Southern Oscillation

Corresponding author address: Dr. William M. Gray, Department of Atmospheric Science, Colorado State University, Fort Collins, CO 80523.

(ENSO). The QBO is represented by three predictors: 50-mb zonal winds, 30-mb zonal winds, and the absolute vertical shear of these two layers. ENSO is included in the forecast scheme as two predictors: the eastern equatorial Pacific sea surface temperature anomaly (SSTA) and the normalized Darwin-to-Tahiti pressure difference (i.e., Southern Oscillation index or SOI). Regional-scale predictive factors also related to ENSO include the 200-mb zonal-wind anomaly (ZWA) and sea level pressure anomalies (SLPA) in the Caribbean basin. The two remaining predictors include West African rainfall in the western Sahel during June and July and in the Gulf of Guinea region during the previous August–November period. The strong concurrent association between western Sahelian rainfall and Atlantic basin intense hurricane activity has been recognized only recently (Gray 1990; Landsea 1991; Landsea and Gray 1992; Landsea et al. 1992).

Indexes of seasonal TC activity include the incidence of named storms (NS), named storm days (NSD), hurricanes (H), hurricane days (HD), intense hurricanes (IH), intense hurricane days (IHD), and hurricane destruction potential (HDP). Precise definitions of each of these indexes are provided in the Appendix. Updated values for these seven indexes of Atlantic basin TC activity for the years 1950–90 are given in Table 1 of Gray et al. (1992c). The data were compiled from Jarvinen et al. (1984) and Neumann et al. (1987). Although 1 August is two months into the official Atlantic basin hurricane season, the early season months of June and July contribute little toward the total seasonal TC activity. Only 9.4% of the NSD, 5.5% of the HD, and 1.6% of the IHD (see Fig. 1) historically occur by the end of July (Landsea 1991). Additionally, unusually high or low amounts of June and July TC activity have little relation to the season as a whole.

This study involves the application of statistical techniques for the development of accurate, independent (jackknifed) 1 August hindcasts for each of the seven measures of seasonal TC activity. We begin by describing the predictive indexes and review the physical processes whereby they affect TC activity on seasonal time scales. A discussion of our methods of analysis includes a description of the forecast equations and supporting statistical studies. The comparative advantages obtained from least sum of absolute deviations (LAD) regression over ordinary least sum of square deviations (OLS) regression are described in section 4; the major findings of the statistical studies are contained in Table 6. A final illustration summarizing the remarkable forecasting capability of the derived relationships is presented in Fig. 11.

2. Meteorological parameters related to Atlantic basin seasonal tropical cyclone activity

A number of pre-August meteorological parameters have been observed to be related to variations in Atlantic basin TC activity occurring after 1 August. These predictive parameters are 1) three measures of the stratospheric QBO zonal winds near 10°N latitude, 2) two measures of West African rainfall, 3) two measures of ENSO, and 4) SLPA and ZWA. Figure 2 shows the geographical distribution of these predictive parameters.

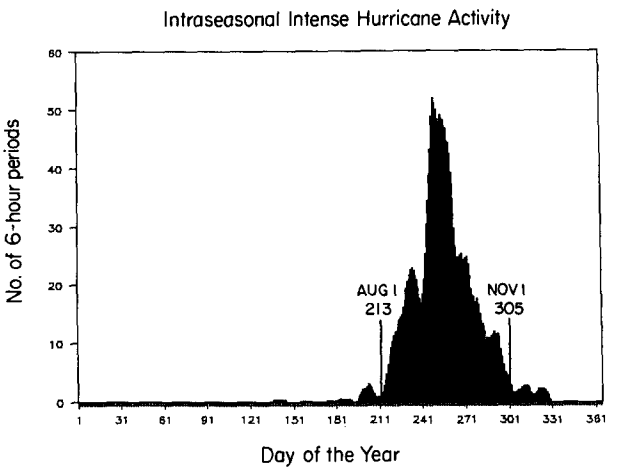

FIG. 1. Plot of Julian Day versus IH activity (9-day running mean) using data for 1986–1989. Note that nearly all IH activity occurs between 1 August (Julian Day 213) and 1 November (Julian Day 305).

Predictive associations based on these parameters are as follows.

a. The stratospheric QBO

Strong stratospheric QBO easterly winds and strong lower-stratospheric vertical wind-shear conditions inhibit lower-latitude TC formation and intensification (Gray 1984a,b; Shapiro 1989). We find that there are only one-half as many Atlantic basin IHD during those seasons when strong easterly stratospheric winds and strong lower-stratospheric vertical wind-shear conditions exist (i.e., during the easterly phase of the QBO) than in those years when stratospheric zonal winds and stratospheric vertical wind shear are weak (i.e., the QBO westerly phase). Hence, Atlantic basin TC activity is inversely related to the value of the zonal winds at 50 mb (U_{50}) and at 30 mb (U_{30}), and to the resulting absolute wind shear between these two levels at latitudes near 10°N. Figure 3 contrasts the composited tracks of IH for the 10 QBO west-phase seasons between 1950 and 1990 wherein September 50-mb (20-km) easterly zonal winds [extrapolated from July, the method of extrapolation is detailed in Gray et al. (1992c)] near 10°N were weakest with those 10 seasons when extrapolated September 50-mb easterly zonal winds were the strongest. Figure 3 graphically illustrates that there were 3.5 times as many IHD in the 10 seasons when the 50-mb QBO were weakest (west phase) as

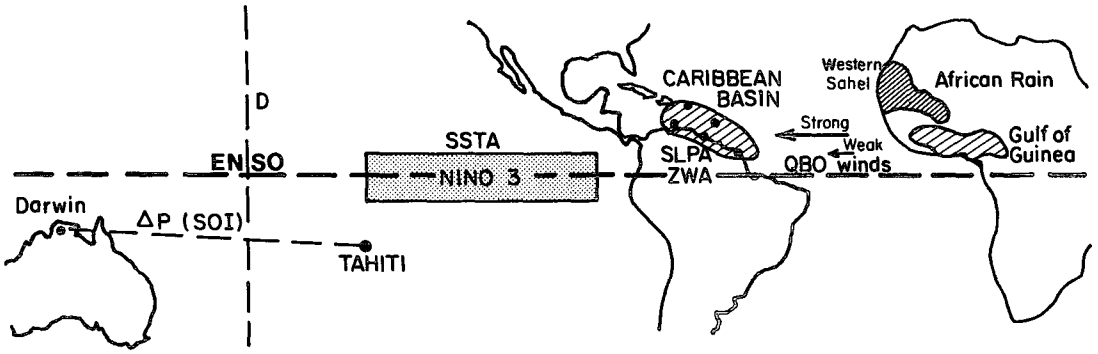

FIG. 2. Locations of areas from which meteorological parameters used in the 1 August Atlantic basin seasonal forecast were derived. The stratospheric QBO is a global-scale tropical phenomena, occurring primarily between ±15° latitude.

when they were strongest (east phase). A similar but smaller modulation of TC activity occurs in seasons of weak versus strong 30-mb (23-km) wind and in seasons of weak versus strong 50-mb–30-mb vertical wind shear (see Table 2). Further discussion on the physical relationship of the QBO to Atlantic TC activity and of the method of extrapolation from observed July data to September conditions are found in Gray et al. (1992c).

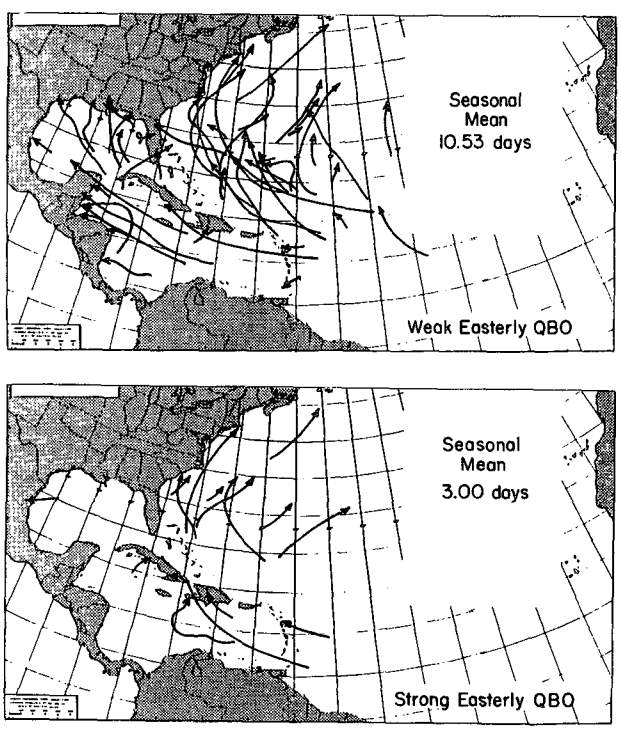

FIG. 3. Contrast of the IH tracks for the 10 seasons between 1950 and 1990 when the two-month extrapolated (July to September) QBO 50-mb zonal-wind speed at 10°N latitude was weakest from the east (upper panel) versus those 10 seasons when the 50-mb wind was strongest from the east (bottom panel). The ratio of difference is 3.51 to 1.

b. West African rainfall

Two prior measures of West African rainfall have a surprisingly strong association with the subsequent seasonal Atlantic basin TC activity occurring after 1 August (Landsea 1991). These two prior predictive signals (see Fig. 4) are

1) Gulf of Guinea rainfall during August–November of the prior year, and
2) western Sahelian rainfall for June–July just preceding the 1 August forecast.

Figure 10 of Gray et al. (1992c) contrasts differences in the IH tracks for seasons following the 10 wettest and the 10 driest previous-year August–November Gulf of Guinea rainfall periods. The ratio of IHD for wet versus dry Gulf of Guinea conditions is 4.17 to 1. It is surprising indeed that rainfall that occurs 8–13 months earlier in an area south of the Sahel could be so closely related to IH activity in the following season. Note that this rainfall has been little affected by the persistent long-term Sahelian drought. Figure 5 portrays a similar

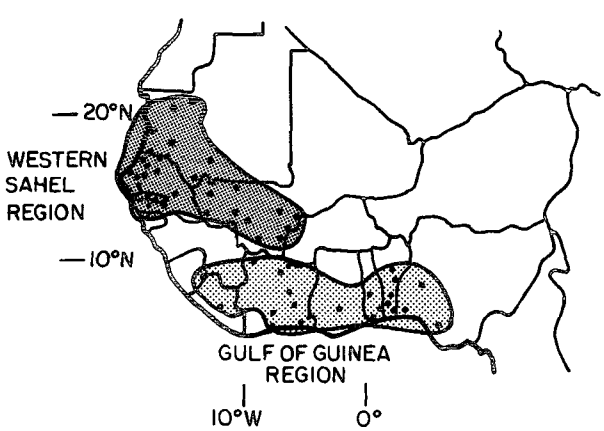

FIG. 4. Locations of rainfall stations that make up the western Sahelian (R_S) and Gulf of Guinea (R_G) precipitation indices (from Landsea 1991).

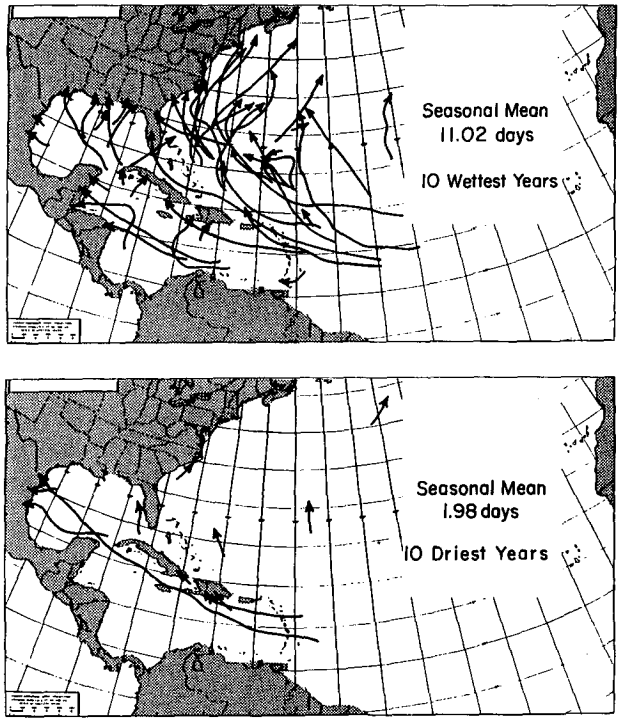

FIG. 5. Contrasting composites of IH tracks during seasons following the 10 wettest (upper panel) versus the 10 driest (bottom panel) June–July periods in the western Sahel between 1950 and 1990. The ratio of IHD between the two composites is 5.57 to 1.

contrast of IH tracks for seasons following the 10 wettest versus the 10 driest June–July western Sahelian precipitation amounts. Here the wet-to-dry ratio of IHD is slightly stronger by a ratio of 5.57 to 1. These two West African rainfall measurements offer unusually strong predictive signals for Atlantic basin TC activity.

c. *El Niño–Southern Oscillation*

Typically, less Atlantic basin TC activity occurs in those hurricane seasons when warm SSTA conditions exist in the eastern Pacific (e.g., an El Niño event) and, hence, when the associated SOI is negative. By contrast, TC activity tends to be enhanced when a cold La Niña event is in progress and thus when positive SOI conditions are present. We can compare TC activity in seasons with anomalously negative SSTA conditions in the Niño 3 (Fig. 2) region of the eastern Pacific (from Wright 1984; Weare 1986) and (typically) positive values of the SOI to seasons with the opposite conditions of warm SSTA and (typically) negative SOI. The track composites in Fig. 6 show a greater than 2 to 1 ratio increase in Atlantic basin IH activity for those ten seasons between 1950 and 1990 when the SOI in June–July was highest versus the 10 seasons during this period when the SOI was lowest. Similar variations occur for those 10 seasons of highest negative versus 10 seasons of highest positive Niño 3 SSTA (not shown).

d. *Sea level pressure anomalies and upper-tropospheric zonal-wind anomalies in the Caribbean basin*

Variable Caribbean basin June–July surface pressure and upper-level (~200-mb) zonal winds also have a profound influence on Atlantic basin TC activity. Figure 7 contrasts the composite of IH tracks, which occurred in the 10 seasons between 1950 and 1990, with the lowest values of Caribbean basin June–July SLPA (see Fig. 2) versus the 10 seasons of highest SLPA; a 3.10 to 1 ratio of IHD is observed. A similar 10-season stratification for June–July low- and high-value 200-mb ZWA (Fig. 8) shows an even stronger modulation (3.76 to 1). Obviously, June–July SLPA and ZWA values should be taken into account when estimates are made of the amount of TC activity to occur after 1 August.

e. *Summary of parameters*

Table 1 lists yearly values of these nine candidate 1 August predictive parameters between 1950 and 1990. Table 2 provides a summary of the ratios of the 10

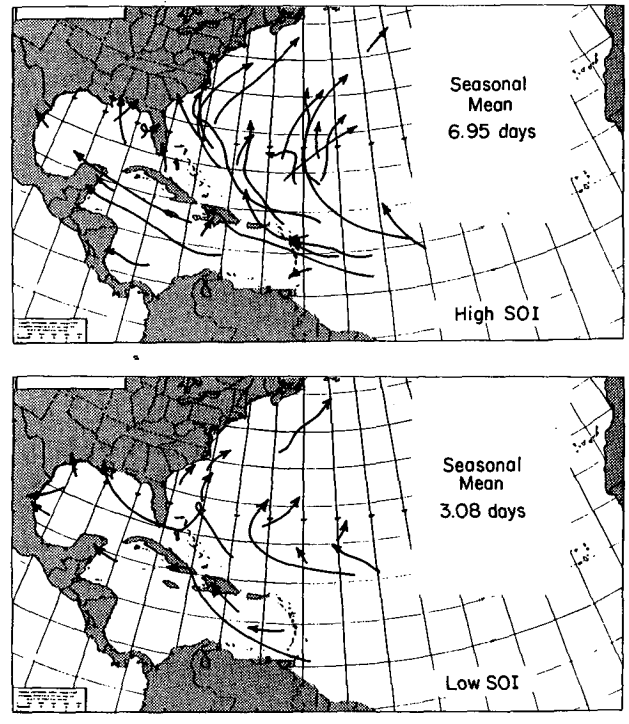

FIG. 6. Contrast of composite IH tracks during the 10 seasons between 1950 and 1990 when the SOI in June–July was the highest (upper panel) versus those 10 seasons when the June–July SOI was the lowest (bottom panel). The ratio of IHD between the two composites is 2.26 to 1.

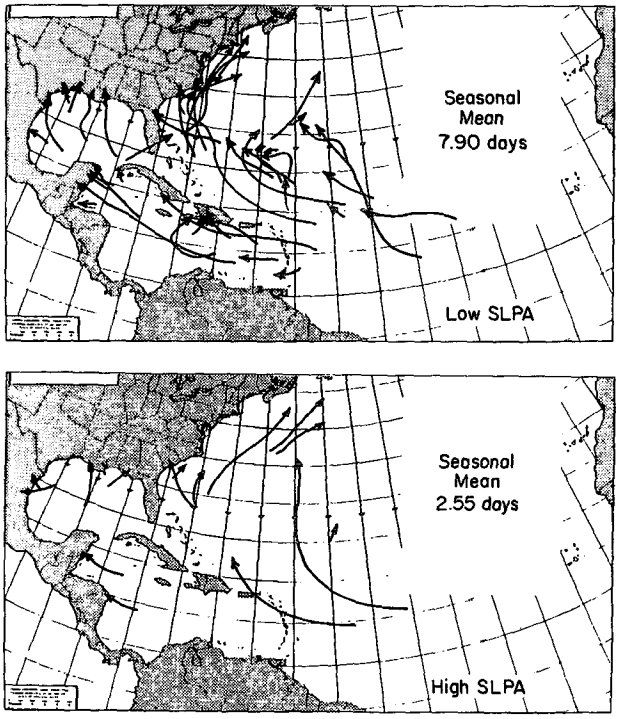

FIG. 7. Contrast of composite IH tracks during the 10 seasons between 1950 and 1990 when the Caribbean basin SLPA in June–July was lowest (upper panel) versus the 10 seasons when SLPA was the highest (bottom panel). The ratio of IHD between the two composites is 3.10 to 1.

highest to the 10 lowest values (or vice versa) for each of these nine predictive parameters and seven measures of seasonal TC activity. While the most prominent differences occur for the seasonal incidence of IHD, a smaller but quite significant modulation is also observed for the other six seasonal measures of TC activity. Table 3 shows which years were selected for each 10-year stratification. Table 4 shows the Pearson product–moment correlation coefficients (r) for each of the nine predictors with the seven measures of seasonal TC activity. West African rainfall offers the best predictive signal, and QBO is the second best predictor. The ENSO predictors are the weakest.

Each of the nine predictors listed in Table 2 shows a measure of predictive accuracy. However, each predictor is not independent of the other predictors. Experimentation with all nine predictors has shown that we improve our forecast accuracy by including all of the predictors, regardless of their degree of interdependence with each other.

3. How predictors influence cyclone activity

The physical processes whereby these large-scale climate controls act to alter Atlantic seasonal TC activity appear to manifest themselves by either enhancing or reducing late August through early October vertical wind shear through the troposphere and lower stratosphere within the western tropical Atlantic and the Caribbean basin. During an average season, upper-tropospheric westerly winds and vertical wind-shear conditions in the tropical Atlantic and Caribbean basin in late August through early October are typically too strong to support very much TC activity. African wave-spawned tropical depressions, which are candidates for TC development, typically undergo upper-level shear action, and do not form into named storms. The few that do become NS seldom become IH. Active TC seasons occur when both the tropical Atlantic and Caribbean basin upper-tropospheric westerly winds are weaker than average (i.e., have easterly upper-level zonal-wind anomalies) and when lower-stratosphere easterly winds near 10°–15°N are weaker than normal (i.e., in relative westerly phase). Seasonal variation in Atlantic TC activity can best be understood by studying the conditions that cause the vertical profile of zonal winds to deviate from mean conditions of late August to early October. As discussed in previous papers (Gray 1984a,b, 1988; Gray et al. 1992c), seasonal values of tropospheric and lower-stratospheric vertical wind shear play a fundamental role in determining the ultimate intensity a developed hurricane can attain and to some degree whether TC activity can form. Figure 9 (adapted from Gray 1990) portrays the typical late

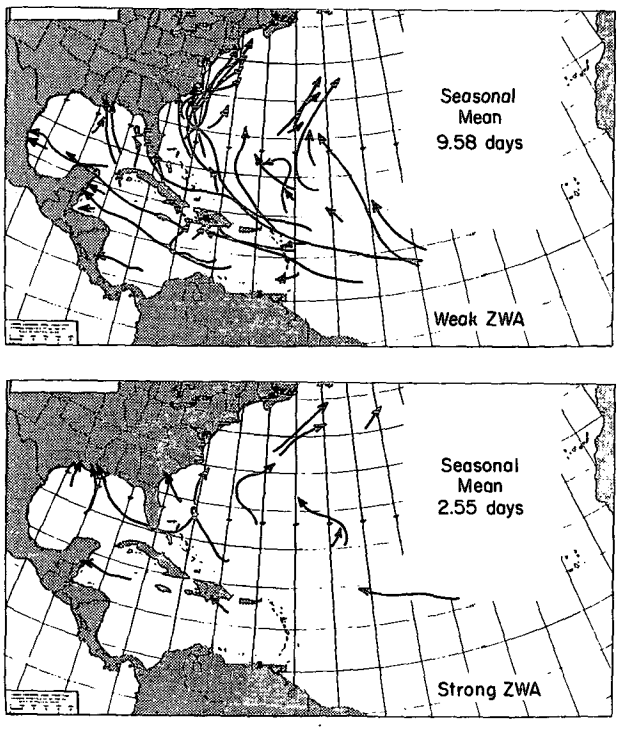

FIG. 8. Contrast of composite IH tracks during the 10 seasons with the lowest June–July 200-mb Caribbean basin ZWA (upper panel) versus the 10 seasons with highest ZWA (bottom panel). The ratio of IHD between the two composites is 3.76 to 1.

TABLE 1. Specific values of nine predictors for each year from 1950 through 1990 used to make the 1 August forecasts of subsequent seasonal TC activity. Data in columns 4, 5, and 8 are expressed in terms of standardized deviations. Note that data in columns 6, 7, and 9 are departures from the long-term (1950–1990) means.

	September (estimated) QBO zonal wind at 10°N—(m s^{-1})			Observed rainfall		Observed Caribbean basin		Observed ENSO	
Year	1 50 mb	2 30 mb	3 Absolute shear |50–30 mb|	4 Western sahelian (std. dev.) June–July	5 Gulf of Guinea previous yr (std. dev.) Aug–Nov.	6 SLPA (mb) June–July	7 ZWA (m s^{-1}) June–July	8 SOI (std. dev.) June–July	9 SSTA (°C) June–July
1950	0	−1	1	0.35	1.07	−0.3	−2.5	2.1	−0.74
1951	−4	−16	12	−0.16	−0.66	−0.6	0.0	−0.7	0.94
1952	−25	−14	11	0.61	0.65	0.0	−2.5	0.5	−0.18
1953	−3	−14	11	0.87	0.41	−0.2	0.0	−0.2	0.56
1954	−22	−32	10	0.63	−0.16	−0.8	−3.0	0.0	−1.14
1955	−2	−2	0	1.44	0.64	−0.7	−5.2	1.5	−1.00
1956	−17	−28	11	0.06	0.41	0.2	−0.7	1.1	−0.66
1957	−6	−6	0	0.13	−0.36	−0.4	3.0	0.0	1.14
1958	−9	−25	16	0.34	1.03	−0.4	−4.5	0.2	0.53
1959	−12	−2	10	−0.32	−0.74	0.1	2.5	−0.5	−0.10
1960	−12	−29	17	0.73	0.12	−0.3	−3.8	0.1	−0.10
1961	−3	0	3	0.89	1.05	0.3	−1.0	−0.2	0.02
1962	−22	−26	4	−0.12	−0.74	0.2	−3.5	0.2	−0.20
1963	−22	−10	12	−0.01	0.73	−0.1	−1.5	−0.6	0.51
1964	0	−11	11	0.92	1.18	−0.9	−2.2	0.5	−0.70
1965	−11	−29	18	−0.11	−0.68	0.2	2.5	−1.5	1.06
1966	−8	−7	1	−0.45	−0.17	−1.0	−3.5	0.0	0.24
1967	−5	−18	13	0.41	−0.14	−0.5	−1.4	0.3	0.05
1968	−16	−32	16	−0.29	−0.51	1.0	−1.0	0.8	0.25
1969	−3	−4	1	0.56	1.28	−0.8	−3.5	−0.4	0.83
1970	−14	−24	10	−0.29	−0.31	−0.1	−2.1	0.1	−0.78
1971	−6	−5	1	−0.33	−0.23	0.5	1.4	0.2	−0.41
1972	−13	−25	12	−0.75	−0.40	0.0	5.1	−1.4	1.21
1973	−5	−7	2	−0.50	−0.88	−0.2	2.2	0.8	−0.88
1974	−13	−27	14	−0.42	0.43	0.4	2.8	0.6	−0.29
1975	−10	−6	4	0.63	−0.08	0.5	−0.7	1.6	−0.81
1976	−3	−18	15	−0.45	−0.55	1.0	2.4	−0.6	0.60
1977	−22	−27	5	−0.77	−0.59	0.5	−0.7	−1.5	0.20
1978	−2	−7	5	0.16	−0.50	0.3	−0.7	0.5	−0.29
1979	−7	−27	20	0.40	−0.73	0.4	−3.6	0.9	0.44
1980	−5	−6	1	−0.90	0.55	0.3	1.2	−0.3	0.65
1981	−7	−24	17	−0.07	0.36	0.1	0.2	1.0	−0.03
1982	−22	−19	3	−0.37	−0.93	0.5	2.8	−1.8	0.96
1983	−5	−20	15	−0.77	−0.61	−0.5	1.7	−0.5	1.39
1984	−20	−31	11	−0.47	−1.32	−0.3	−1.1	−0.4	−0.75
1985	−3	−2	1	−0.27	0.04	0.6	2.0	−0.6	−0.70
1986	−5	−23	18	−0.86	0.13	1.2	3.6	0.5	−0.10
1987	−25	−26	1	−0.51	−0.48	−0.5	4.4	−1.8	1.43
1988	−3	−19	16	−0.17	1.37	0.1	−10.3	0.4	−1.95
1989	−14	−27	13	0.87	0.35	0.6	0.5	0.7	−0.18
1990	−6	−5	1	−0.53	0.19	0.0	1.0	0.3	0.18

August to early October vertical profile of zonal wind at latitudes of 10°–15°N in the western Atlantic. Curve a shows mean conditions in the troposphere, and curve c shows easterly stratospheric QBO conditions. Curves b and d show the typical zonal winds in those seasons with enhanced TC activity. Active TC seasons require favorable deviations from the climatological curve.

All of the seasonal predictors have some influence on the alteration of the late August to early October vertical profile of zonal winds. Figure 10 portrays how the various June–July predictors cause late August to early October zonal winds to vary in the troposphere and lower stratosphere. Western Sahelian drought and warm ENSO conditions during late August to early October act to enhance vertical wind shear in the troposphere. Wet western Sahelian rainfall conditions and cold ENSO conditions occur in conjunction with favorable upper-tropospheric easterly wind anomalies.

a. QBO influence

As discussed in Gray et al. (1992c), lower-stratospheric QBO winds play an important role in seasonal

TABLE 2. Ratios for each of seven indexes of TC activity for those years comprising the 10 highest yearly values versus the 10 lowest yearly values for each of the nine predictor indices occurring during the 41-year period from 1950 through 1990. For example, the ratio of HDP for the 10 most westerly QBO years to the 10 most easterly QBO years is 2.48, as shown in the upper right of the array.

	Corresponding ratio of TC activity						
Predictor index	NS	NSD	H	HD	IH	IHD	HDP
U 50-mb QBO							
10 low/10 high	1.57	1.97	1.60	2.10	3.29	3.51	2.48
U 30-mb QBO							
10 low/10 high	1.48	1.96	1.66	1.69	2.53	1.63	1.83
U 50–30 mb—shear							
10 low/10 high	1.46	1.64	1.50	1.62	1.68	1.36	1.59
Western Sahelian rain—June–July							
10 high/10 low	1.45	1.65	1.47	1.93	3.33	5.57	2.39
Gulf of Guinea rain—Aug.–Nov.							
10 high/10 low	1.52	1.86	1.78	2.42	2.94	4.17	2.85
SLPA—June–July							
10 low/10 high	1.21	1.43	1.27	1.68	2.27	3.10	1.97
ZWA—June–July							
10 low/10 high	1.54	1.75	1.78	2.22	3.08	3.76	2.62
SOI—June–July							
10 high/10 low	1.39	1.52	1.29	1.49	1.76	2.26	1.68
SSTA—June–July							
10 low/10 high	1.35	1.32	1.25	1.35	1.75	1.95	1.46

TC modulation. When QBO winds are strongly from the east (i.e., the easterly phase upper portion of Fig. 9—curve c), stratosphere to troposphere wind shear is high, and penetrative convection into the lower stratosphere, or the influences of such convection (gravity waves, cumulus upward propagation of momentum, etc.), tends to be sheared and ventilated away to the west in relation to the traveling system. This condition is in contrast to conditions of weak stratosphere easterly flow (relative westerly phase—curve d), where convective influences upon the lower stratosphere can be maintained over the lower system. Additionally, there are systematic height and temperature field differences in the lower stratosphere and upper troposphere associated with the east and west phases of the QBO. These hydrostatic variations, as discussed in Gray et al. (1992a,b), tend to favor deep convective systems at latitudes of 8°–18°N during west QBO years and to inhibit deep convection at these latitudes in east QBO years.

Seasonal TC activity is thus enhanced in westerly QBO situations and suppressed in easterly conditions. In the forecasting scheme, the July stratosphere zonal-wind data is used to estimate the QBO winds that occur two months later during the height of the hurricane season.

TABLE 3. Listing of the 10 highest and the 10 lowest years for each predictor used to compute the ratios in Table 2.

Predictive parameter	10 high years	10 low years
1. Extrapolated QBO U_{50}	1952, 54, 56 ,62, 63 1968, 77, 82, 84, 87	1950, 53, 55, 61, 64 1969, 76, 78, 85, 88
2. Extrapolated QBO U_{30}	1954, 56, 60, 65, 68 1974, 77, 79, 84, 89	1950, 55, 59, 61, 69 1971, 75, 80, 85, 90
3. Extrapolated QBO $\lvert U_{50}-U_{30}\rvert$	1958, 60, 63, 65, 68 1979, 81, 83, 86, 88	1950, 55, 57, 66, 69 1971, 80, 85, 87, 90
4. Western Sahelian rain June–July	1952, 53, 54, 55, 60 1961, 64, 69, 75, 89	1966, 72, 73, 76, 77 1980, 83, 84, 86, 87
5. Gulf of Guinea rain Aug.–Nov. (previous year)	1950, 52, 55, 58, 61 1963, 64, 69, 80, 88	1951, 59, 62, 65, 73 1979, 82, 83, 84, 87
6. Caribbean SLPA June–July	1968, 71, 74, 75, 76 1977, 82, 85, 86, 89	1951, 54, 55, 57, 58 1964, 67, 69, 83, 87
7. ZWA–Caribbean June–July	1957, 59, 65, 72, 73 1974, 76, 82, 86, 87	1950, 54, 55, 58, 60 1962, 66, 69, 79, 88
8. SOI June–July	1950, 55, 56, 68, 73 1975, 79, 81, 88, 89	1951, 63, 65, 72, 76 1977, 82, 83, 85, 87
9. SSTA (eastern Pacific) June–July	1951, 57, 65, 69, 72 1976, 80, 82, 83, 87	1950, 54, 55, 64, 70 1973, 75, 84, 85, 88

b. West African rainfall influence

There is a strong statistical relationship between western Sahelian rainfall and Caribbean basin upper-tropospheric zonal winds during the height of the hurricane season in September (Landsea and Gray 1992). Upper-tropospheric zonal winds are typically weak westerlies or actual easterlies during times of heavy western Sahelian rainfall, and inversely, there are typically strong westerly winds during western Sahelian drought conditions. The circulation conditions that bring about western Sahelian drought and heavy rainfall are also the same conditions that are associated with positive or negative upper-level zonal-wind deviations in the latitude belt of 10°–15°N.

Two processes are envisaged as acting to cause West African rainfall to have a lagged relationship to the following season's Atlantic TC activity. Heavier June–July western Sahelian rainfall is a response to an early establishment of a strong monsoon trough. This rainfall is hypothesized to lead to earlier vegetation growth and

TABLE 4. Pearson product–moment correlation coefficients (r) for each of the seven measures of seasonal TC activity with each of the nine seasonal predictors.

	NS	NSD	H	HD	IH	IHD	HDP
1. QBO 50 mb	−0.46	−0.54	−0.41	−0.46	−0.48	−0.36	−0.45
2. QBO 30 mb	−0.51	−0.57	−0.54	−0.53	−0.50	−0.36	−0.49
3. shear	−0.20	−0.21	−0.29	−0.24	−0.18	−0.12	−0.19
4. Western Sahelian	0.39	0.53	0.39	0.52	0.64	0.71	0.60
5. Gulf of Guinea	0.51	0.60	0.57	0.59	0.67	0.63	0.63
6. SLPA	−0.33	−0.38	−0.31	−0.39	−0.41	−0.37	−0.40
7. ZWA	−0.38	−0.33	−0.35	−0.40	−0.45	−0.45	−0.44
8. SOI	0.29	0.38	0.31	0.33	0.36	0.30	0.35
9. SSTA	−0.34	−0.19	−0.20	−0.18	−0.22	−0.21	−0.19

greater amounts of soil moisture and evapotranspiration in the following August and September period. This extra moisture source appears to lead to a higher percentage of stronger and more concentrated waves coming off of West Africa. Thus, interannual variability of easterly waves and the general circulation over the Atlantic appears to be the mechanism that ties the western Sahelian rainfall to Atlantic TC activity. This has been more thoroughly discussed by Gray and Landsea (1991), Landsea (1991), and Landsea and Gray (1992). The physical mechanisms likely linking previous-year Gulf of Guinea rainfall to Atlantic TC activity are discussed in Gray et al. (1992c).

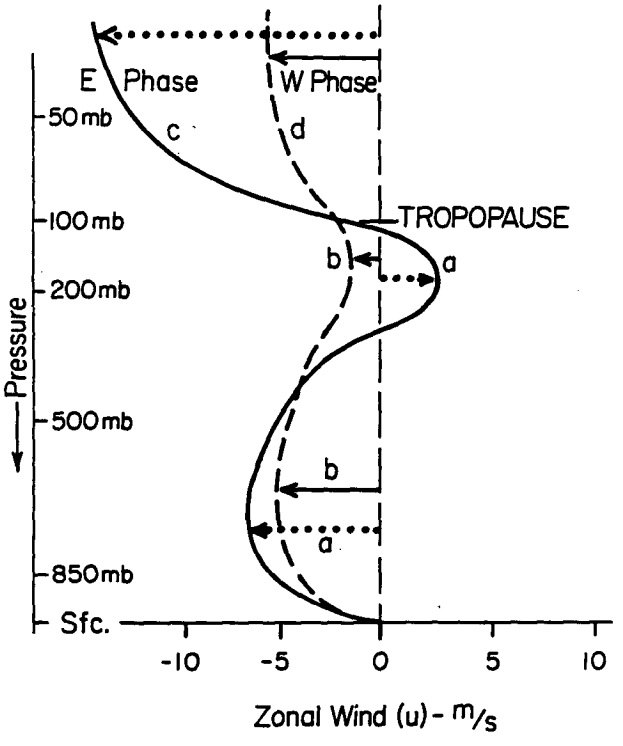

FIG. 9. Portrayal of climatological vertical profiles of zonal-wind conditions in the tropical (10°–15°N) western Atlantic and eastern Caribbean basin from late August to early October (curve a) and of easterly QBO conditions (curve c). The dashed line shows the favorable tropospheric zonal-wind deviation from climatology and westerly phase QBO conditions that are required for the most active TC seasons. Curves c and d illustrate the east- and west-phase QBO conditions in the stratosphere [Adapted from Gray (1990)].

c. *ENSO*

As discussed by Arkin (1982), Gray (1984a), Shapiro (1987), and Gray and Sheaffer (1991), there is a strong relationship between ENSO, Caribbean basin, and tropical Atlantic upper-tropospheric zonal winds. In those seasons in which high values of the eastern Pacific SSTA or low values of the SOI occur, the Caribbean basin and tropical Atlantic typically have positive ZWA. This inhibits Atlantic TC activity. Opposite or weak upper-tropospheric zonal winds occur in those

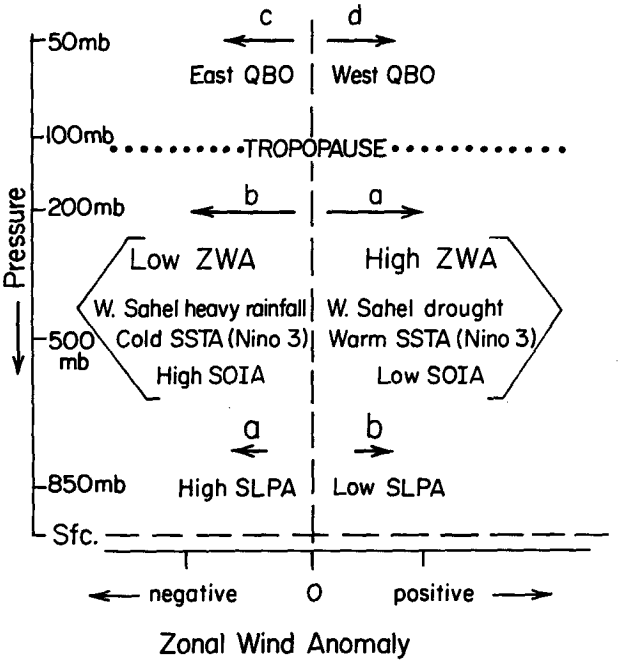

FIG. 10. Schematic summary of how the various predictors cause the zonal-wind profile of Fig. 9 to vary. Active seasons have negative zonal-wind deviations in the upper troposphere but positive deviations in the lower stratosphere and lower troposphere.

seasons of cold eastern Pacific SSTA and high SOI. Tropical cyclone activity is usually enhanced during these latter conditions. The use of June–July SSTA and SOI represents a persistence forecast that typically carries over to the August through early October period. Of course, if drastic changes were to occur in ENSO between the two time periods, this will likely cause a loss of forecasting skill.

d. Caribbean basin sea level pressure and upper-tropospheric conditions

The Caribbean basin appears to have a degree of independent influence on seasonal TC activity. There are August–September periods when the intertropical convergence zone (ITCZ) in the Caribbean basin and in the northern part of South America is found farther north or farther south of its average position. When the ITCZ is farther north of its normal position, SLPA and ZWA are typically negative. When the ITCZ is farther south of its normal position, positive surface pressure and positive upper-level wind anomalies typically occur at the same time. The former conditions enhance and the latter conditions suppress Atlantic basin TC activity. Ray (1935), Brennan (1935), Shapiro (1982), and Gray (1984b) have also discussed the predictive association of western Atlantic surface pressure on TC frequency variation.

4. Analyses and results

Once the predictors for each of the three predictive indexes (QBO, West African rainfall, and ENSO combined with SLPA and ZWA) have been selected, the statistical methodology consists of four distinct but interrelated steps. 1) An objective least sum of absolute deviations (LAD) regression procedure based on the $n = 41$ years in question yields estimated LAD regression coefficients for the constant and each of the nine predictors. The weights associated with each of the three predictive indexes are obtained from the proportionate contribution of the estimated LAD regression coefficients associated with the predictors in each index. Separate sets of index weights are obtained for each of the seven dependent variables (NS, NSD, H, HD, IH, IHD, HDP). Consequently, the forecast model for each of the seven dependent variables is a linear model consisting of a constant and three predictive indexes (the weights for each index being objectively obtained fixed values). In the construction of any forecast model, it is imperative that the model be developed on a subset of the data and then independently tested on a different subset of the data that was not used in the formation of the model. This cross-validation of a forecast model may be accomplished by means of a jackknife procedure. 2) A cross-validation (jackknife) procedure ensures that the prediction for any year is independent of the predictor observations for that year. Since the purpose of the present methodology is to forecast a single year, 40 years of data (i.e., $n - 1 = 41 - 1$) are used for the formulation of each forecast model, and each model is then tested on the remaining one year of independent data not used in the construction of the model. This procedure is repeated 41 times, yielding 41 prediction values for each of the seven seasonal dependent variables. 3) The cross-validated prediction values and the observed values for each of the $n = 41$ years are compared by calculating a measure of agreement. 4) The probability of the measure of agreement is obtained under the null hypothesis. Finally, a prediction equation is constructed for the following (42d) year. In this prediction of a forthcoming hurricane season, no information is available on the independent variables at the time of the prediction. Consequently, in a forecast of an upcoming season, a nonjackknife procedure is used. Note that this nonjackknife procedure corresponds exactly with the jackknife procedure used for the 41 years: in the case of the 41 years, information on the independent variables for each of the years in question is known, but is not considered. In the case of the 42d year, the information is not known, and therefore not considered. Since any one of the 41! orderings of 41 years yields the same result, the procedure is not affected by a serial correlation. In addition, tests to detect first-order serial correlations among the temporally ordered residuals (i.e., the year-to-year differences between predicted and observed values) were not significant for each of the seven seasonal dependent variables in question. Details of this statistical methodology are presented in appendix B of Gray et al. (1992c).

The prediction equation for each of the seven seasonal dependent variables (i.e., NS, NSD, H, HD, IH, IHD, HDP) is

$$\hat{y} = \hat{\beta}_0 + \hat{\beta}_1 W + \hat{\beta}_2 R + \hat{\beta}_3 E, \qquad (1)$$

where $\hat{y}$ represents one of the seven dependent variables; $\hat{\beta}_0$, $\hat{\beta}_1$, $\hat{\beta}_2$, and $\hat{\beta}_3$ are the LAD regression weights determined from a nonjackknifed solution (Gray et al. 1992c, see appendix B); W is a composite function of QBO data involving extrapolated (July) zonal winds at 50 mb (U_{50}) and 30 mb (U_{30}), where

$$W = a_1 U_{50} + a_2 U_{30} + a_3 |U_{50} - U_{30}|; \qquad (2)$$

R is a composite function of West African rainfall data involving June–July western Sahelian (R_S) and previous year August–November Gulf of Guinea (R_G) rainfall, where

$$R = a_4 R_S + a_5 R_G; \qquad (3)$$

and E is a composite function of Caribbean basin and ENSO data involving the sea level pressure anomaly in the lower Caribbean basin for June and July, the zonal-wind anomaly in the Caribbean basin for June and July, the standardized Tahiti-minus-Darwin sea level pressure difference anomaly for June and July,

TABLE 5. Empirical weights for composite functions of QBO, African rainfall, and Caribbean basin–ENSO data for the jackknifed LAD regression procedure prediction equations.

	QBO			Rainfall		Caribbean basin–ENSO			
	a_1	a_2	a_3	a_4	a_5	a_6	a_7	a_8	a_9
NS	1.000	0.711	−0.082	1.000	−1.260	1.000	0.106	−0.275	0.046
NSD	1.000	0.560	−0.358	1.000	1.109	1.000	0.096	−0.864	−1.489
H	1.000	1.928	0.284	1.000	17.876	1.000	−1.172	−1.966	−0.025
HD	1.000	0.894	0.266	1.000	0.613	1.000	0.182	−0.050	−0.075
IH	1.000	0.614	−0.467	1.000	0.591	1.000	0.051	0.474	0.630
IHD	1.000	0.730	2.777	1.000	0.248	1.000	−0.019	1.272	0.567
HDP	1.000	0.608	0.629	1.000	0.256	1.000	0.169	0.705	0.312

and the sea surface temperature anomaly in Niño 3 for June and July, where

$$E = a_6(SLPA) + a_7(ZWA) + a_8(SOI) + a_9(SSTA). \quad (4)$$

The weights (a_1, a_2, a_3, a_4, a_5, a_6, a_7, a_8, and a_9) for each of the predictor variables are given in Table 5 for each of the dependent variables. The weights in this paper were objectively obtained with an algorithm due to Barrodale and Roberts (1974) for each of the seven dependent variables using the LAD nongrouped nonjackknifed 10-parameter prediction model. While the predictor variables are associated with the composite functions W, R, and E, where W and R comprise the 1 December prediction model (Gray et al. 1992c), choices other than W, R, and E might have yielded similar results (alternative composite functions were not investigated). If y and $\hat{y}$ denote the observed and predicted dependent variables, respectively, then the agreement coefficient (ρ) is defined by

$$\rho = (\mu_\delta - \delta)/\mu_\delta,$$

where $\delta = 1n^{-1} \sum_{i=1}^{n} |y_i - \hat{y}_i|$ and μ_δ is the average value of δ over all $n!$ equally likely permutations of $y_1, \ldots, y_n$ relative to $\hat{y}_1, \ldots, \hat{y}_n$ under the null hypothesis that the n ($n = 41$) pairs (y_i and $\hat{y}_i$ for $i = 1, \ldots, n$) are merely the result of random assignment (Gray et al. 1992c; Mielke 1984, 1991).

The agreement coefficients ρ and their associated probability values P are given in Table 6. (Note that P is commonly called a P value, i.e., the probability of a random value being as or more extreme than the observed value under the null hypothesis.) For comparative purposes only, the corresponding values of the squared Pearson product-moment correlation coefficient r^2 are presented in the last column of Table 6. Since the results of Table 6 are based on the cross-validated (jackknifed) LAD regression criterion, the values of r^2 are not maximized. While ρ is a measure of agreement and $\rho = 1$ implies that all observed and predicted value pairs fall on a line with unit slope that passes through the origin, r^2 is strictly a measure of linearity (i.e., $r^2 = 1$ implies that all observed and predicted value pairs fall on a line that does not necessarily have a unit slope or pass through the origin). Thus, the values of r^2 are often larger than the corresponding values of ρ. Since r^2 depends on squared Euclidean distance residual values, r^2 can also be smaller than ρ (Mielke 1984, 1991). The fact remains that r^2 is not a satisfactory measure of agreement.

TABLE 6. Agreement coefficient ρ, probability P, and r^2 values from a jackknifed LAD regression procedure.

	ρ	P	r^2
NS	0.447	0.33×10^{-6}	0.433
NSD	0.608	0.14×10^{-8}	0.584
H	0.472	0.48×10^{-6}	0.455
HD	0.505	0.23×10^{-6}	0.558
IH	0.618	0.25×10^{-8}	0.677
IHD	0.617	0.50×10^{-9}	0.598
HDP	0.556	0.12×10^{-7}	0.584

The influence of the jackknife procedure on both the measure of agreement ρ and the squared Pearson product-moment correlation coefficient r^2 is now examined. Suppose 1) ordinary least sum of square deviations (OLS) regression is used instead of LAD regression, and/or 2) nongrouped (NG) prediction models are used instead of grouped (G) prediction models (i.e., nongrouping or grouping of the independent variables of the prediction model). The a priori empirical weights for each group in a 1 August LAD grouped jackknifed prediction model are obtained from the corresponding LAD nongrouped nonjackknifed prediction model. (An analogous approach is used for all OLS grouped jackknifed prediction models.) Specifically, the grouped version of the 1 August prediction model consists of a constant value and three predictive indexes (associated with composite functions W, R, and E). While the constant value is the single value 1, the values of the predictive index associated with composite function W (i.e., a_1, a_2, and a_3) are fixed prior to the jackknife procedure. (The same holds for the values associated with composite functions R and E.) Thus, only four parameters (β_0, β_1, β_2, and β_3) are estimated with the jackknife procedure for the 1 August

TABLE 7. Measures of agreement ρ between observed and predicted values associated with nonjackknifed and both grouped (G) and nongrouped (NG) jackknifed LAD and OLS regression procedures.

	NS	NSD	H	HD	IH	IHD	HDP
LAD regression model:							
1 December forecast results							
Nonjackknifed	.440	.514	.447	.493	.498	.451	.457
Jackknifed—G	.440	.514	.447	.491	.498	.451	.447
Jackknifed—NG	.411	.386	.279	.305	.376	.374	.235
1 August forecast results							
Nonjackknifed	.447	.608	.472	.516	.618	.617	.557
Jackknifed—G	.447	.608	.472	.505	.618	.617	.556
Jackknifed—NG	.186	.435	.256	.210	.544	.499	.325
OLS regression model:							
1 December forecast results							
Nonjackknifed	.359	.407	.388	.400	.491	.450	.430
Jackknifed—G	.308	.359	.339	.355	.448	.403	.385
Jackknifed—NG	.244	.306	.280	.300	.408	.367	.338
1 August forecast results							
Nonjackknifed	.435	.528	.428	.489	.605	.579	.531
Jackknifed—G	.374	.477	.367	.432	.562	.529	.476
Jackknifed—NG	.270	.388	.247	.330	.490	.450	.379

grouped prediction model. In contrast, all 10 parameters are estimated with the jackknife procedure for the 1 August nongrouped prediction model. The results of this study are presented in Tables 7 and 8 for both the 1 December (Gray et al. 1992c) and the 1 August predictions. The highest r^2 values are achieved by the nonjackknifed OLS regression model. However, the highest r^2 values for jackknifed models are achieved by the grouped jackknifed LAD regression model for all 14 cases in Table 8. These findings were unanticipated. In contrast, the highest ρ values are achieved by the nonjackknifed LAD regression model, and the highest ρ values for jackknifed models are achieved by the grouped jackknifed LAD regression model for all 14 cases in Table 7. The jackknifed results for the nongrouped LAD and OLS regression models are much worse for all 28 cases than the corresponding grouped LAD and OLS regression model results in Tables 7 and 8. These findings suggest that the grouped LAD regression models are exceptionally stable for routine applications. The fact that such problems occur with OLS regression should not be surprising. Sheynin (1973) has shown that C. F. Gauss introduced OLS regression as an alternative to LAD regression (which was previously considered by D. Bernoulli, R. J. Boscovich, and P. S. Laplace) simply because Gauss was unable to implement the linear programs he developed for LAD regression (appropriate computational equipment did not exist at the time).

In order to predict future results, regression weights

TABLE 8. Squared Pearson product-moment correlation coefficients r^2 between observed and predicted values associated with nonjackknifed and both grouped (G) and nongrouped (NG) jackknifed LAD and OLS regression procedures.

	NS	NSD	H	HD	IH	IHD	HDP
LAD regression model:							
1 December forecast results							
Nonjackknifed	.395	.488	.466	.514	.581	.517	.544
Jackknifed—G	.395	.488	.466	.511	.581	.517	.527
Jackknifed—NG	.368	.358	.280	.320	.415	.431	.276
1 August forecast results							
Nonjackknifed	.433	.584	.455	.573	.677	.598	.585
Jackknifed—G	.433	.584	.455	.558	.677	.598	.584
Jackknifed—NG	.164	.436	.198	.198	.593	.509	.302
OLS regression model:							
1 December forecast results							
Nonjackknifed	.416	.523	.482	.538	.585	.543	.570
Jackknifed—G	.313	.434	.391	.464	.502	.454	.495
Jackknifed—NG	.202	.347	.299	.378	.433	.399	.423
1 August forecast results							
Nonjackknifed	.527	.649	.511	.597	.711	.668	.643
Jackknifed—G	.406	.564	.399	.504	.646	.577	.556
Jackknifed—NG	.255	.430	.154	.321	.528	.449	.394

TABLE 9. Regression weights for the nonjackknifed (LAD) regression procedure prediction equations.

	$\hat{\beta}_0$	$\hat{\beta}_1$	$\hat{\beta}_2$	$\hat{\beta}_3$
NS	11.228	0.100	−0.757	−0.931
NSD	68.890	1.029	5.106	−5.309
H	7.410	0.046	0.050	0.239
HD	33.509	0.493	4.503	−4.318
IH	3.459	0.041	1.142	−0.677
IHD	5.023	0.055	6.370	−1.217
HDP	93.364	1.756	31.814	−14.372

($\hat{\beta}_0$, $\hat{\beta}_1$, $\hat{\beta}_2$, and $\hat{\beta}_3$) are required. Using 1) the index weights for the predictor variables (a_1, a_2, a_3, a_4, a_5, a_6, a_7, a_8, and a_9), 2) LAD regression, and 3) a nonjackknifed solution, the regression weights are calculated. Table 9 gives the LAD regression coefficients for each dependent variable for future predictions. Substituting (2), (3), and (4) into (1) yields the prediction equation given by

$$\hat{y} = \hat{\beta}_0 + \hat{\beta}_1(a_1U_{50} + a_2U_{30} + a_3|U_{50} - U_{30}|) + \hat{\beta}_2(a_4R_S + a_5R_G) + \hat{\beta}_3[a_6(SLPA) + a_7(ZWA) + a_8(SOI) + a_9(SSTA)]. \quad (5)$$

As an example of the seasonal forecasts, the coefficients of Tables 5 and 9 yield the following prediction equation for the seasonal number of IH:

$$IH = 3.459 + 0.041(1.0U_{50} + 0.614U_{30} - 0.467|U_{50} - U_{30}|) + 1.142(1.0R_S + 0.591R_G) - 0.677[1.0(SLPA) + 0.051(ZWA) + 0.474(SOI) + 0.630(SSTA)]. \quad (6)$$

Note in Table 6 that we can independently (jackknife) hindcast over 44% of the measure of agreement coefficient ρ for all seven dependent variables. In fact, we can hindcast over 60% of the value of ρ for the seasonal numbers of NSD, IH, and IHD. The probability that there is no hindcast statistical skill in any of these dependent variables is between 10^{-6} and 10^{-10}.

5. Discussion

Figure 11 portrays the very large differences in observed IH tracks when composites are drawn for the 10 calmest IH and IHD hindcasts versus the 10 most active IH and IHD hindcasts. Note the large variations in observations for these extreme hindcasts. These results indicate that it is possible to make seasonal forecasts by 1 August that are considerably more skillful than what could be expected using climatology alone as a predictor. (Climatology as a predictor yields values of the agreement coefficient close to 0, which indicates no prediction skill.) If atmospheric variability remains within the same modes it has occupied over the last 41 years, then vastly improved future seasonal forecasts are available. We have no reason for thinking that the atmosphere will not behave during the next few decades as it has during the last four decades. The existence of such strong seasonal predictive relationships was not expected. It is remarkable that Atlantic seasonal TC activity, manifesting itself as multiple sporadic mesoscale events, would show such a strong lag response to forcing functions far removed in space and time.

Since the initial half of the 41 years in question involved a very active TC period, whereas the last half involved an extremely mild period, the resulting prediction equation accounts for both of these distinctly different periods and hopefully will provide reasonable predictions for a broad spectrum of TC activity in the future. The incisive concerns by individuals such as Ramage (1983) regarding the effects of "siege-of-time" on long-term predictions have been seriously considered in the present effort. Current research is focusing on the implications of long-period seasonal-prediction degradation.

A major observation is the fact that efficient cross-validated results are attainable with the coupling of LAD regression and appropriate a priori groupings of predictor variables. The common attempt to use OLS regressions as a tool for cross-validation (i.e., the predicted values are independent of the observed values) appears hopeless, as indicated by the empirical results.

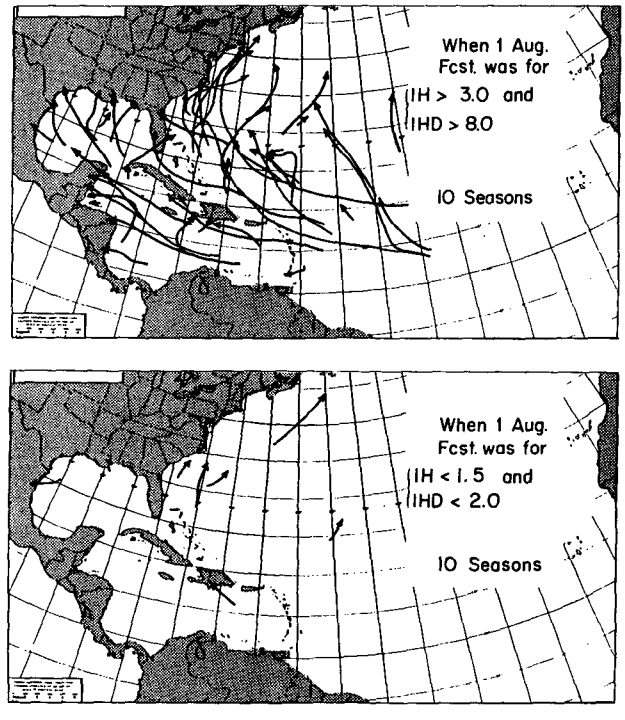

FIG. 11. Contrast of the observed IH tracks from the 10 most active hindcast (IH > 3.0 and IHD > 8.0) seasons versus the 10 calmest hindcast seasons (IH < 1.5 and IHD < 2.0).

The problem appears to be the counterintuitive properties associated with the fact that the squared residuals of OLS regression operate in a nonmetric space (Mielke 1984, 1991). Also, because the squared Pearson product–moment correlation coefficient 1) does not measure agreement between the observed and predicted values ($r^2 = 1$ does not imply a unit slope or a zero intercept) and 2) is dependent on the counterintuitive nonmetric nature of squared residuals, the use of r^2 should be avoided. Rather, the chance-corrected Euclidean distance-based measure of agreement ρ does have reasonable properties for the present purpose.

It is likely that even greater forecast accuracy can be obtained through additional statistical analyses and with the inclusion of other forecast parameters not yet studied. New research is pursuing ideas that will improve forecast skill by 1 June, the official starting date of the Atlantic hurricane season. It follows that increased skill earlier on may provide improvements to be made on the current forecast scheme discussed here.

Acknowledgments. The authors wish to thank Richard Taft and William Thorson for their very expert assistance in the processing of large amounts of meteorological data necessary to make this forecast, and to John D. Sheaffer for his many beneficial comments. Barbara Brumit and Laneigh Walters provided expert assistance in manuscript preparation and data analysis. This research was supported primarily by a climate grant from the National Science Foundation and the NOAA Office of Global Programs. The authors are appreciative of the very constructive comments by the reviewers.

APPENDIX

Definitions

Atlantic basin: the area including the entire North Atlantic Ocean, the Caribbean Sea, and the Gulf of Mexico.

Tropical cyclone (TC): a large-scale circular flow occurring within the tropics and subtropics that has its strongest winds at low levels, including hurricanes, tropical storms, and other weaker rotating vortices.

Tropical storm: a tropical cyclone with maximum sustained winds between 18 and 32 m s^{-1}.

Named storm (NS): a hurricane or a tropical storm.

Named storm day (NSD): four 6-h periods during which a tropical cyclone is observed or estimated to have attained tropical storm or hurricane intensity winds.

Hurricane (H): a tropical cyclone with sustained low-level winds of 33 m s^{-1} or greater.

Hurricane day (HD): four 6-h periods during which a tropical cyclone is observed or estimated to have hurricane intensity winds.

Intense hurricane (IH): a hurricane reaching at some point in its lifetime a sustained low-level wind of at least 50 m s^{-1}. This constitutes a category 3 or higher on the Saffir–Simpson scale (Simpson 1974).

Intense hurricane day (IHD): four 6-h periods during which a hurricane has intensity of Saffir–Simpson category 3 or higher.

Hurricane destruction potential (HDP): a measure of a hurricane's potential for wind and storm-surge destruction defined as the sum of the square of a hurricane's maximum wind speed for each 6-h period of its existence. Values are given in 0.25×10^4 (m s^{-1})^2.

Saffir–Simpson (S–S) category: A measurement scale (1–5) of a hurricane's wind and ocean-surge intensity. The weakest hurricane is 1; the most intense hurricane is 5 (Simpson 1974).

REFERENCES

Arkin, P. A., 1982: The relationship between interannual variability in the 200 mb tropical wind field and the Southern Oscillation. *Mon. Wea. Rev.*, **110**, 1393–1401.

Barrodale, I., and F. D. K. Roberts, 1974: Solution of an overdetermined system of equations in the l_1 norm. *Commun. Assoc. Comp. Mach.*, **17**, 319–320.

Brennan, J. F., 1935: Relation of May–June weather conditions in Jamaica to the Caribbean tropical disturbances of the following season. *Mon. Wea. Rev.*, **63**, 13–14.

Chan, J. C. L., 1991: Prediction of seasonal tropical cyclone activity over the Western North Pacific. Preprints, *The Fifth Conf. on Climate Variations*, Denver, Amer. Meteor. Soc., 521–524.

Gray, W. M., 1984a: Atlantic seasonal hurricane frequency: Part I: El Niño and 30 mb quasi-biennial oscillation influences. *Mon. Wea. Rev.*, **112**, 1649–1668.

——, 1984b: Atlantic seasonal hurricane frequency: Part II: Forecasting its variability. *Mon. Wea. Rev.*, **112**, 1669–1683.

——, 1988: Environmental influences on tropical cyclones. *Aust. Meteor. Mag.*, **33**, 127–139.

——, 1990: Strong association between west African rainfall and U.S. landfalling intense hurricanes. *Science*, **249**, 1251–1256.

——, and C. W. Landsea, 1991: Predicting U.S. hurricane spawned destruction for West African rainfall. *13th Annual National Hurricane Conf.*, Miami, 40 pp.

——, and J. Sheaffer, 1991: El Niño/Quasi-Biennial Oscillation influence on seasonal Atlantic hurricane activity. *ENSO Teleconnections Linking World Wide Climate Anomalies: Scientific Basis and Societal Impact*, M. H. Glantz, R. W. Katz, and N. Nicholls, Eds., Cambridge University Press, 257–283.

——, ——, and J. A. Knaff, 1992a: Hypothesized mechanism for stratospheric QBO influence on ENSO variability. *Geophys. Res. Lett.*, **19**, 107–110.

——, ——, and ——, 1992b: Influence of the stratospheric QBO on ENSO variability. *J. Meteor. Soc. Japan*, **70**, 975–995.

——, C. W. Landsea, P. W. Mielke, and K. J. Berry, 1992c: Predicting Atlantic seasonal hurricane activity 6–11 months in advance. *Wea. Forecasting*, **7**, 440–455.

Jarvinen, B. R., C. J. Neumann, and M. A. S. Davis, 1984: A tropical cyclone data tape for the North Atlantic basin, 1886–1983: Contents, limitations, and uses. NOAA Tech. Memo. NWS NHC 22, Miami, FL, 21 pp.

Landsea, C. W., 1991: West African monsoonal rainfall and intense hurricane associations. Department of Atmospheric Sciences Paper No. 484, Colorado State University, Ft. Collins, CO, 272 pp.

——, and W. M. Gray, 1992: The strong association between western Sahel monsoon rainfall and intense Atlantic hurricanes. *J. Climate*, **5**, 435–453.

——, ——, P. W. Mielke, Jr., and K. J. Berry, 1992: Long-term variations of western Sahel monsoon rainfall and intense U.S. landfalling hurricanes. *J. Climate*, **5**, 1528–1534.

Mielke, P. W., 1984: Meteorological applications of permutation techniques based on distance functions. *Handbook of Statistics, Vol 4: Nonparametric Methods,* P. R. Krishnaiah, and P. K. Sen, Eds., North-Holland Publishing Co., 813–830.

——, 1991: The application of multivariate permutation methods based on distance functions in the earth sciences. *Earth-Sci. Rev.,* **31,** 55–71.

Neumann, C. J., B. R. Jarvinen, A. C. Pike, and J. D. Elms, 1987: *Tropical cyclones of the North Atlantic Ocean, 1871–1986.* National Climatic Data Center and National Hurricane Center, 186 pp.

Nicholls, N., 1992: Recent performance of a method for forecasting Australian seasonal tropical cyclone activity. *Aust. Meteor. Mag.,* **40,** 105–110.

Ramage, C. S., 1983: Teleconnections and the siege of time. *J. Climatol.,* **3,** 223–231.

Ray, C. L., 1935: Relation of tropical cyclone frequency to summer pressures and ocean surface-water temperatures. *Mon. Wea. Rev.,* **63,** 10–12.

Shapiro, L. J., 1982: Hurricane climate fluctuations. Part II: Relation to large-scale circulation. *Mon. Wea. Rev.,* **110,** 1014–1023.

——, 1987: Month-to-month variability of the Atlantic tropical circulation and its relationship to tropical storm formation. *Mon. Wea. Rev.,* **115,** 2598–2614.

——, 1989: The relationship of the quasi-biennial oscillation to Atlantic tropical storm activity. *Mon. Wea. Rev.,* **117,** 1545–1552.

Sheynin, O. B., 1973: R. J. Boscovich's work on probability. *Arch. Hist. Exact Sci.,* **9,** 306–324.

Simpson, R. H., 1974: The hurricane disaster potential scale. *Weatherwise,* **27,** 169 and 186.

Weare, B. C., 1986: An extension of an El Niño index. *Mon. Wea. Rev.,* **114,** 644–647.

Wright, P. B., 1984: Relationships between indices of the Southern Oscillation. *Mon. Wea. Rev.,* **112,** 1913–1919.